HIGHLY SENSITIVE STRAIN GAUGE BASED ENTIRELY ON ELASTOMERS VIA MOLDING PROCESS

BY

CHI LU

THESIS

Submitted in partial fulfillment of the requirements
for the degree of Master of Science in Materials Science and Engineering
in the Graduate College of the
University of Illinois at Urbana-Champaign, 2012

Urbana, Illinois

Adviser:

Professor John A. Roger

ABSTRACT

This thesis is mainly about the research on highly sensitive strain gauges based entirely on elastomers and partially about the molding process which is used to fabricate the strain gauge and pattern poly-dimethylsiloxane (PDMS). In this thesis, I demonstrate the design, fabrication and characterization of high gauge factor (GF), all-elastomer strain gauge systems, with Young's modulus of 224 kPa, which lies within the range of the human epidermis. The devices combine carbon black doped-PDMS resistors, carbon nanotube doped-PDMS conductors and an insulating PDMS matrix/substrate to yield, in mechanically optimized geometrical layouts, desired characteristics. Measurement of strains in human skin using sensor sheets of this type, physically laminated onto the wrist, illustrates a representative implementation. Strains measured in this mode on the wrist are between 11.2% and 22.6%. Such sheets can be readily laminated on and form conformal contact to the human skin, with only modest mechanical constraints on natural motions. Moreover, the devices remain attached even under full-range bending of the joint, with minimal effects of mechanical constraint or mass loading.

The approach I used to pattern the conductive PDMS is molding and scrapping. Molding process can not only be used to pattern conductive PDMS but also regular PDMS. For example, skin-like PDMS sheet with an array of hollows will be discussed later in the thesis.

To My Family

ACKNOWLEDGEMENTS

I would not be able to complete this research project without the support of many people. First of all, I would like to express my deepest gratitude to my advisor, Professor John A. Rogers who admitted me into his group when I was a freshmen in college. Professor Roger's knowledge and accomplishments in the field of flexible electronics inspired my research career in UIUC and motivate me for the future career. His enthusiasm for research and diligent attitude toward his career have been the driven force for my progress. His perspective into problems and creative thinking are competences that I cannot stop learning from him.

The undergraduate and graduate programs of Materials Science and Engineering in UIUC are highly recognized by peers, and this is due to all the professors' dedication to their research and their efforts on teaching. I did learn a lot from them; without their sharing of knowledge, I would not be able to be who I am now.

Special thanks to my group members: Prof. Nanshu Lu, Dr. Alfred Baca, Dr. Andrew P. Bonifas, Lizhi Xu, Ming Ying, Abid Ameen, and so on. Their assistance and collaboration with me helped me to complete my projects. Nanshu Lu led me into the experimental world and taught me not only knowledge but also skills on experiments, and also I would like to thanks her for the collaboration on the paper we submitted together. Alfred Baca was the first person who taught me how to do micro-fabrication when I was just an inexperienced first-year undergrad. Andrew Bonifas provides me suggestions when I encounter obstacles on experiments. Lizhi and Ming assist me on problem solving, fabrication, and so on. Abid assist me significantly on the measurements of strain gauges. I thank all other group members and officemates for sharing the literature and invaluable discussions.

I highly appreciated the trainings and generous help Shang Tao, Bharat Sankaran, and Tony Bank in the Frederick Seitz Materials Research Laboratory (MRL) at UIUC. MRL also provides fantastic laboratory facilities without which the experimental work could not have been accomplished.

I would also like to convey thanks to UIUC MSE and NSF for providing the financial means.

TABLE OF CONTENTS

CHAPTER 1

INTRODUCTION

1.1 WHAT IS STRAIN GAUGE?

Strain gauges are devices used to measure the change of shapes of objects. Their applications span from structural health monitoring in civil engineering [1] to implantable strain sensors in biomedical engineering [2]. Most commonly used strain gauges are made out of metallic foils supported by an insulating backing and their gauge factor is typically around two.

A wire strain gauge can effectively measure strain in only one direction; it can be defined as:

$$\varepsilon = \frac{l - l_0}{l_0} \times 100\% = \frac{\Delta l}{l_0} \times 100\% \quad (1).$$

However, to determine the three independent components of plain strain, three linearly independent measurements of strain are needed, i.e. three strain gauges positioned in a rosette-like layout [3]. Consider a strain rosette attached on the surface with an angle α from the x-axis as shown in Figure 1.1(a) [3]. In Figure 1.1(a), the rosette contains three stain gauges with an angle β next to the angle α and an angle γ on the other side of the angle β. Suppose that the strain measured from these three strain gauges are ε_a, ε_b, and ε_c, respectively, then the following transformation equation in coordinate system can be used to convert the longitudinal strain from each strain gauge into stain expressed in x-y coordinates,

$$\varepsilon_{x'} = \frac{\varepsilon_x + \varepsilon_y}{2} + \frac{\varepsilon_x - \varepsilon_y}{2}\cos 2\theta + \varepsilon_{xy}\sin 2\theta \qquad (2).$$

Applying Eq. (2) to each of the three strain gauges, the following results can be obtained:

$$\varepsilon_a = \frac{\varepsilon_x + \varepsilon_y}{2} + \frac{\varepsilon_x - \varepsilon_y}{2}\cos 2\alpha + \varepsilon_{xy}\sin 2\alpha \qquad (3.1)$$

$$\varepsilon_b = \frac{\varepsilon_x + \varepsilon_y}{2} + \frac{\varepsilon_x - \varepsilon_y}{2}\cos 2(\alpha + \beta) + \varepsilon_{xy}\sin 2(\alpha + \beta) \qquad (3.2)$$

$$\varepsilon_c = \frac{\varepsilon_x + \varepsilon_y}{2} + \frac{\varepsilon_x - \varepsilon_y}{2}\cos 2(\alpha + \beta + \gamma) + \varepsilon_{xy}\sin 2(\alpha + \beta + \gamma) \qquad (3.3).$$

Using all Eq. (3.1) to (3.3), unknowns ε_x, ε_y, and ε_{xy} can be solved. Now, consider two special cases. Case 1: a 45° strain rosette aligned with both x and y axes, i.e. $\alpha = 0$, and $\beta = \gamma = 45°$, as shown in Figure 1.1(b) [3]. In this case, Eq. (3.1) to (3.3) can be simplified as following:

$$\varepsilon_x = \varepsilon_a \qquad (4.1)$$

$$\varepsilon_y = \varepsilon_c \qquad (4.2)$$

$$\varepsilon_{xy} = \varepsilon_b - \frac{\varepsilon_a + \varepsilon_c}{2} \qquad (4.3).$$

Case 2: a 60º strain rosette, the middle one is aligned with the *y*-axis, i.e., $\alpha = 30º$, $\beta = \gamma = 60º$, as shown in Figure 1.1(c) [3]. Again, Eq. (3.1) to (3.3) can be modified as:

$$\varepsilon_x = \frac{2}{3}\left(\varepsilon_a - \frac{1}{2}\varepsilon_b + \varepsilon_c\right) \tag{5.1}$$

$$\varepsilon_y = \varepsilon_b \tag{5.2}$$

$$\varepsilon_{xy} = \frac{1}{\sqrt{3}} - \left(\varepsilon_a - \varepsilon_c\right) \tag{5.3}.$$

1.2 STRAIN GAUGE FACTOR

Deformations in the object lead to deformations in the foil are causing its electrical resistance to change. The fractional change in resistance, $\Delta R / R_0$, is related to the mechanical strain ε by the gauge factor (*GF*):

$$GF = \frac{\Delta R / R_0}{\varepsilon} \tag{6}.$$

The *GF* for metallic foils are typically between 2 to 5 [4], due mostly to changes in length and cross-sectional area. A simple formulation assuming constant resistivity and constant volume yields $R/R_0 = (L/L_0)^2$ [5]. Since $R/R_0 = 1+\Delta R/R_0$ and $L/L_0 = 1+\varepsilon$, when $\varepsilon << 1$, $\Delta R/R_0 \approx 2\varepsilon$, which corresponds to $GF = 2$.

Compared to metallic foils, semiconductor devices can exhibit much larger *GF* due to piezoresistive effects. Here, the resistivity changes rapidly with strain due to the dependence of the bandgap on inter-atomic spacing [6-8]. For example, the gauge factor of p-type [110] single crystalline silicon can be as high as 200 [6, 9, 10]. As a result, for precision measurements,

semiconductor gauges, also called piezoresistors, are preferred over metal foils. These types of devices are widely used as 'hard' sensors attached to stiff materials such as metals, concretes and high modulus plastics for structural health monitoring or quantifying specimen deformation. Recent work shows that ultrathin sheets of single crystalline silicon, i.e. nanomembranes [11], can yield similar types of devices in flexible form on thin plastic substrates [12].

1.3 WHEATSTONE BRIDGE

In addition to longitudinal and transverse straight resistors, Wheatstone bridges are also commonly integrated into strain gauges to measure the change of electrical properties of device due to the deformation. The results in this thesis are mostly performed by the Wheatstone bridge. A diagram of basic Wheatstone bridge is shown in Figure 1.2. The circuit consists of four identical resistors, so that ideally the output voltage, $V_o = V_{ac}$ would be zero. When the device is stretched in the direction parallel to R_2 and R_4 in Figure 1.2, R_2 and R_4 will get stretched and R_1 and R_3 will get compressed due to Poisson's effect.

To calculate the actual value of R_1, R_2, R_3, and R_4, the unstrained value of the strain gauge, R_0, and the gauge factor, GF, must be known. Therefore, the relationship between resistance and the applied strain, ε, will become:

$$R_1 = R_3 = R_0 + \Delta R_1\left(1 + \Delta R_1 / R_0\right) = R_0\left(1 + GF_1\varepsilon\right) \quad (7).$$

$$R_2 = R_4 = R_0 + \Delta R_2\left(1 + \Delta R_2 / R_0\right) = R_0\left(1 + GF_2\varepsilon\right) \quad (8).$$

Moreover, it is known that

$$V_0 = V_a - V_c \tag{9}$$

$$V_a = V_{dc}\left(\frac{R_1}{R_1 + R_4}\right) \tag{10}$$

$$V_b = V_{dc}\left(\frac{R_2}{R_2 + R_3}\right) \tag{11}$$

Therefore,

$$V_0 = V_{dc}\left[\frac{R_1}{R_1 + R_4} - \frac{R_2}{R_2 + R_3}\right] = V_{dc}\left[\frac{R_0\varepsilon\left(GF_1 - GF_2\right)}{R_0\left[\left(1 + GF_1\varepsilon\right) + \left(1 + GF_2\varepsilon\right)\right]}\right] \tag{12}$$

1.4 STRAIN GAUGES USED ON HUMAN BODY MEASUREMENTS

In order to study biomechanics, physiology, and kinesiology, devices that can conform to the curvilinear surfaces of biological tissues and also accommodate the large deformations associated with them are required. Ordinary strain gauges made out of silicon slabs are clearly unsuitable for such uses, but neither are flexible devices (metal foils or silicon nanomembranes) due to their inability to wrap complex curved objects or to stretch (i.e. respond in a reversible manner to strains much larger than ~1%). Electrogoniometers and electrotorsiometers made of metal wires can be mounted on human joints to measure, in a bending mode, motions such as human elbow rotation and ankle dorsiflexion, but they cannot map spatial distributions of strain, and they also impose unacceptably large mechanical constraints for measuring motions of soft parts of the body, such as the skin [13, 14]. Mercury-in-rubber strain gauges [15] represent one solution, suitable for monitoring blood flow and tissue swelling by local measurements of skin extension. The filling requirements in the fabrication of such devices, however, restrict their

geometries and modes of use. For instance, most devices provide only single measurement capabilities in closed loop form for application around approximately cylindrical parts of the body such as toes or legs [15]. Other approaches include platinum (Pt)-based strain gauges for integration onto surfaces of objects such as contact lenses to record changes in the curvature of the cornea for the diagnosis of glaucoma [16]. These and other efforts establish a trend in strain gauge development toward increasingly soft and deformable mechanics, for bio-integrated applications. To monitor the surface strains of human skin due to joint motion, tissue swelling, wound healing, or even emotional expression, a sheet of skin-like, highly sensitive strain gauges that can be directly applied onto the tissue surface would be ideal. Such a system could conformally laminate onto the curvilinear surfaces of human body without any mechanical fixturing or adhesives and with an ability to follow the natural motions of the tissue without delaminating or imposing any mechanical constraint, similar to recently described 'epidermal' electronic systems [17].

1.5 Figures

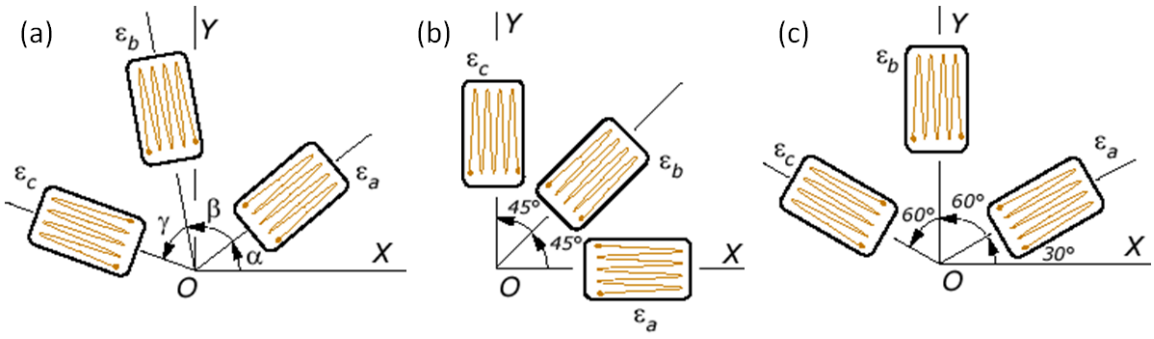

Figure 1.1: Different setups of strain rosette: (a) a strain rosette attached on the surface with an angle α from the x-axis, and internal angles β and γ, (b) a special case of (a) in which α = 0, and β = γ = 45°, and (c) another special case of (a) in which α = 30º, β = γ = 60º. [3]

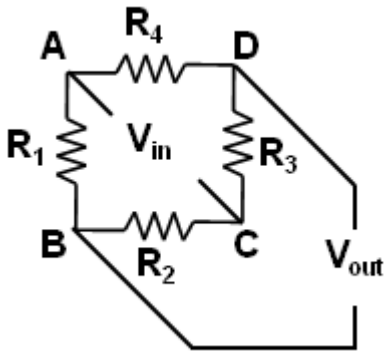

Figure 1.2: Schematic of a basic Wheatstone bridge.

CHAPTER 2

ELECTRICALLY CONDUCTIVE RUBBERS

2.1 ADVANTAGES OF USING ELECTRICALLY CONDUCTIVE RUBBERS

Traditionally, electronic sensors are made of hard materials such as metals and semiconductors. However, if versatile applications are desired, such as sensors on the clothes, organisms, and etc., increasing the stretchability and bendability of sensors would be necessary. Moreover, for biomedical applications, strain gauges attached to ligaments or skins should be soft enough so that it will not affect the original dynamics of the tissue. Therefore, soft materials such as polymers would be a natural solution. Taking the advantage of electrically conductive elastomers, it is possible to develop soft and conformable strain gauges. Electrically conductive rubber (ECR) is a promising class of material for this purpose, due to its intrinsically low modulus, low density, elastic mechanics and its pronounced piezoresistivity [18, 19].

2.2 TYPES OF ELECTRICALLY CONDUCTIVE RUBBERS

ECRs can be prepared by dispersing conductive fillers such as carbon black (CB), carbon nanotubes (CNT) or metallic nanoparticles (e.g. gold nanoparticles, silver nanoparticles, and etc.) into elastomers such as poly(dimethylsiloxane) (PDMS) [19-21]. Molding and curing processes can be used to manipulate such materials, which people refer to generally as conductive PDMS (CPDMS), into desired geometries for device integration [22, 23, 24]. The

electrical behaviors of CPDMS, such as the conductivity and the piezoresistance, depend strongly on filler concentration and morphology (e.g. particle size and structure) as well as filler–filler and filler–matrix interactions [19, 25, 26]. With similar levels of loading, the sheet resistances of CB-doped PDMS (CB-PDMS) are several orders of magnitude higher than those of PDMS doped with multi-walled CNTs (CNT-PDMS) [19, 26]. The piezoresistive effect is believed to arise from the different compressibilities between the filler and the matrix, such that the application of stress changes in the separations between individual filler elements [27-29]. Applications of these effects range from tactile sensors [24, 30-32] to strain gauges [18, 33] and flow sensors [34]. Examples of CPDMS-based soft strain gauges include knee-mounted electrogoniometers that use CNT-PDMS [18] and 'tattoo-like', epidermal strain gauges based on CB-PDMS [17]. The former devices are attractive, in part, because they are capable of measuring deformations as large as 280%. Relatively low *GFs* (~0.3) and requirements for bandages and/or adhesives to facilitate mounting on the human body [18] represent disadvantages. CB-PDMS gauges supported by polyimide and interconnected with serpentine metal wires can be integrated with thin (~30 μm), low modulus elastomers (Ecoflex, Smooth-on, Inc.) to form devices that are exceptionally compliant, with mechanical properties approaching those of the skin itself. An array of such gauges, in the form of thin sheets, can spontaneously and reversibly laminate onto human skin, with the capability for quantifying and spatially mapping distributions of strain. A key drawback is that the overall gauge factor is compromised by the underlying polyimide layer [17], which limits the magnitude of deformation in the CB-PDMS. In addition to CPDMS, conductive fillers can be mixed into different rubbers for various purposes, for instance, Ecoflex, which provides lower modulus. There are also commercially available conductive rubbers, such as Elastosil® LR3162 A/B produced by Wacker Chemie AG.

CHAPTER 3

FABRICATION

3.1 FABRICATION OF HIGHLY SENSITIVE STRAIN GAUGE

The fabrication procedures appear in Figure 3.1. Two types of CPDMS are prepared: mixing 1. 25 wt% carbon black (VULCAN®XC72R, Carbot Corp.) in one case, and, 2. 15 wt% multi-wall carbon nanotubes (CheapTubes.com) in the other, both with 30:1 (base polymer: curing agent) PDMS (Sylgard® 184 Silicone Elastomer, Dow Corning Corp.) using a drill mixer (DR260B, Black & Decker). Figure 3.1A shows a schematic illustration of the as-fabricated all-elastomer strain gauge, including both CPDMS components in a PDMS matrix. Magnified views corresponding to the area defined by the red dotted box are shown in Figs. 3.1B to 3.1H. Laminating a sheet of polyimide (Kapton® HN, DuPont) onto a glass substrate coated with a thin layer of PDMS cleaned by acetone and isopropanol (IPA) represents the first step.

A positive photoresist (10 μm thick; spin-coated at 800 rpm; AZ 4620P, AZ Electronic Materials Corp.) patterned with trenches defines the geometry of the sensing components, as shown in Fig. 3.1B. Squeeze casting a mixture of uncured CB-PDMS into these trenches with a razor blade and then gently scraping off excess material, leaves the sample in the configuration shown in Fig. 3.1C. Curing the CB-PDMS in a 70 °C oven for 2 hours and then rinsing away the photoresist with acetone yields isolated features for the sensor components of the system, as shown in Fig. 3.1D. Repeating steps B to D creates patterns of thick (20 μm thick; spin-coated at

200 rpm) CNT-PDMS interconnects, as shown in Figs. 3.1E to G. The fabrication procedure can be finalized by involving uniformly spin-casting 30:1 PDMS (~0.3 mm thick) over the entire structure and then curing at 70 °C for 2 hours as shown in Fig. 3.1H. Since PDMS has weak adhesion to polyimide, the integrated system can be peeled away easily, leaving all of the CPDMS structures embedded, as shown in Figs. 3.1I and 3.1A. Ribbon cables, in the form of anisotropic conductive films (ACF, Elform Heat Seal Connectors), attached to ultra-violet ozone (UVO) treated CPDMS pads at the edges of the device, provide means for electrical measurement and evaluation on skin. Here, the cable terminates on a customized printed circuit board with soldered wires that interface to a digital multimeter (DMM, SMU2055, Signametrics Precision Instruments) for resistance or voltage measurement.

3.2 PATTERNING PDMS VIA MOLDING PROCESS

Polydimethylsiloxane (PDMS) elastomers have been widely used in academic and industrial applications because of their unique mechanical, physical, and chemical properties [19]. With the recent development in soft lithography and polymer microelectromechanical system (MEMS), PDMS has been built into a large array of micro- or nano-scale devices for biological and medical applications [19, 35, 36]. Here in this thesis, three types of PDMS are reported. Electrically conductive PDMS for the all-elastomer strain gauges has already been mentioned previously in section 3.1. Later in this section, molding regular PDMS and photopatternable PDMS will be introduced.

A PDMS sheet with an array of hollows is going to be used for real sample demonstration in later sections. This PDMS sheet can be potentially used as backing-substrate for flexible electronics, and also, it is soft enough to be called "skin-like". There are two main purposes of using substrates with hollows. First of all, for epidermal electronics which need to be mounted on the skin, the substrate should be air and moisture permeable; otherwise, delamination would be caused and the device would not function properly. Secondly, the Young's modulus of a sheet with hollows is definitely lower than that of a sheet without hollows for the same material. How much Young's modulus can be reduced can be determined by the ratio of hollow area to the entire area of the sheet. Intuitively, the larger the hollow area is, the lower the Young's modulus. However, in this thesis, I will mainly focus on the fabrication aspect.

3.2.1 Molding PDMS via Photoresist Mold

As mentioned, molding is one of the most commonly used approaches to define the features [35]. Figures 3.2 and 3.3 shows a mold made of photoresist (AZ 40 XT, AZ Electronic Materials Corp., spin-coated at 200 rpm) and a PDMS sheet with an array of hollows fabricated by the photoresist mold. AZ 40 XT is a positive photoresist and the depth of the mold created by this process is about 64 μm. If a thicker mold is desired, AZ 40XT can be used to create molds up to 130 micrometers. Figure 3.4 shows the fabrication procedures of molding PDMS. First of all, a layer of photoresist is spin-coated on the top of a glass slide as shown in Figs. 3.4A and B. To cure the photoresist, the temperature is set at 70 °C initially, then 90 °C, and finally 115 °C for 5 minutes each. The reason of using elevating temperatures to cure the photoresist is to

evaporate the solvent gradually and to avoid the formation of bubbles. Next, photoresist is patterned by UV light and then AZ 300 MIF developer (AZ Electronic Materials Corp.), as shown in Fig. 3.4C. In this example, around 6000 mJ/cm^2 of UV light is applied, and for AZ 40 XT, post exposure bake (30 seconds at 100 °C in this case) is required for this particular photoresist. Since a glass slide is used as substrate here, and both of glass and PDMS are silicon-dioxide based materials; they would bond to each other on the surface gradually, and as a result, the PDMS sheet would not be able to be detached from the glass slide in the end. Therefore, in order to facilitate the release of patterned-PDMS later, a layer of trichlorosilane should be vapor-coated on the top of glass to form a barrier to avoid direct contact of glass and PDMS; this process is as shown in Fig. 3.4D. Afterwards, 30:1 (base polymer: curing agent) PDMS is poured into the mold and gently scraped with razor blade to get rid of excess PDMS, as shown in Figs. 3.4E and F. Next, the PDMS is cured at 70 °C for 2 hours to crosslink. After the photoresist is removed by acetone, PDMS remains as shown in Fig. 3.4G. Fig. 3.4H is the top view of Fig. 3.4G and shows the PDMS sheet with an array of hollows. To pick up the PDMS sheet, PDMS stamp can be used for transfer. Both the PDMS sheet and stamp do not need to be specially treated on the surface for the purpose of transfer because the van der Waals force is sufficient in this case. After the sheet is picked up, it can be transferred to any desired place. For the application of flexible electronics for epidermis, PVA can be a good choice. First, evaporating 4/40 nm of Ti/Au on the PVA as adhesive layer, and then putting the PDMS sheet in the UVO box to destroy chemical bonds on the surface of the PDMS sheet for later adhesion. Next, attaching the PVA sheet to the PDMS sheet and detaching the PDMS sheet from the PDMS stamp. Since PVA is water-soluble, the PVA sheet can be rinsed off by spraying water on it to mount devices on the skin, and ultimately, the PDMS sheet with hollows will be the only

thing left. Compared to photopatternable PDMS, there are more steps involved to the molding approach. However, the feature resolution is better when using the direct molding method.

3.2.2 Photopatternable PDMS

By adding a photoinitiator of 2, 2-dimethoxy-2-phenyl acetophenone (DMAP), which makes PDMS function as a negative photoresist, PDMS pre-polymer will be sensitive to ultraviolet (UV) wavelengths, and then it can be photopatternable [37-40, 41-44]. Exposure to UV light results in PDMS crosslinking and curing [41]. There are commercially available photodefinable silicone products (WL-5000 series, Dow Corning) in the market that use this approach [42-44]. In addition to the products mentioned, another approach to prepare photopatternable PDMS is to use benzophenone as the photoinitiator. [45] Benzophenone is a photosensitizer commonly used to initiate the free-radical polymerization of acrylates and monomers with certain functional group under UV exposure. Researchers have reported its use with siloxane polymers. [46-49] The approach of using photodefinable PDMS can eliminate the need of a master mold and the other issues related to molding. However, it also requires larger amount of exposure under UV light, which means longer exposure time. Figure 3.5 shows the PDMS sheet with hollows made by using photopatternable PDMS. The PDMS presented here was made of 10:1 (base polymer: curing agent) PDMS and 5 wt % (compared to the weight of pre-gel) of benzophenone. Figure 3.6 demonstrates the process of patterning PDMS via photo-sensitive PDMS. First, spin-coating benzophenone-added PDMS on a glass substrate as shown on Figures 3.6A and B. Afterwards, covering the uncured PDMS by mask and exposed under UV light. For the sample shown in the Fig. 3.5, it was exposed to 18,000mJ of UV light.

Afterwards, baking the uncrosslined PDMS bake at 110 °C for 3 minutes to crosslink and cure the part of PDMS that was exposed under UV light as shown in Fig. 3.6C. In the end, putting the sample into toluene to dissolve the uncrosslinked part (the part covered by the mask and is not exposed under UV light). Figure 3.6D shows the final PDMS patterns on the glass substrate and the top view of it.

3.3 Figures

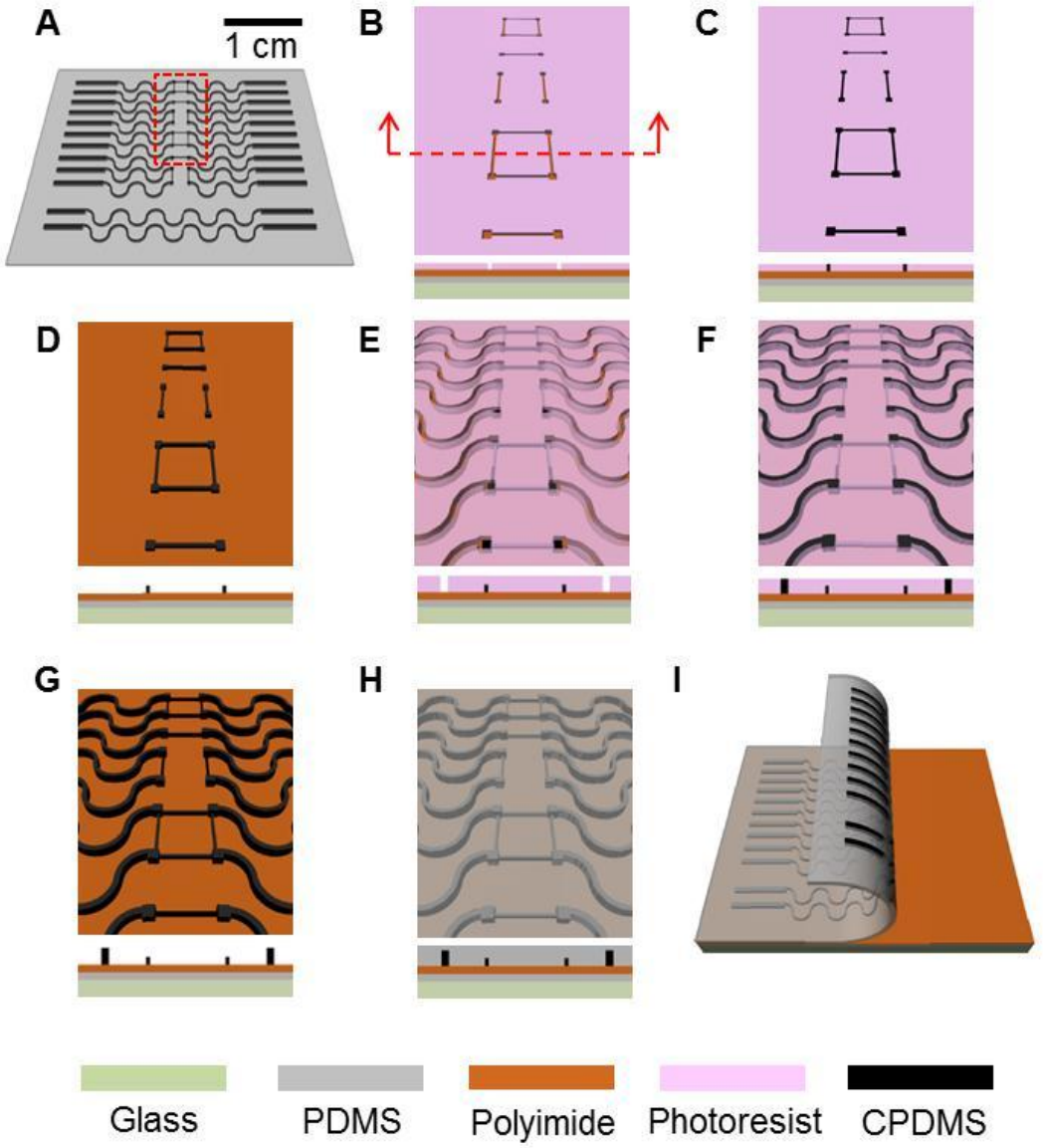

Figure 3.1: Schematic illustrations of fabrication procedures for all-elastomer strain gauges. (A) Full-sized completed device. Tilted top views and cross-sectional views of the red dotted box in Frame A are provided in Frames B through H. (B) Positive photoresist patterned in the form of trenches with layouts matching desired resistors and Wheatstone bridge geometries, on a film of polyimide. (C) CB-PDMS squeezed into the trenches with excess removed by a razor blade. (D) Photoresist rinsed off after curing the CB-PDMS. (E) Thick layer of photoresist patterned in the form of trenches with layouts matching the interconnect wires. (F) CNT-PDMS squeezed into the trenches with excess removed by a razor blade. (G) Photoresist rinsed off after curing the CNT-PDMS. (H) Cast PDMS to cover all of the patterned features. (I) Peeling the entire integrated structure from the polyimide to yield a device shown in Frame A.

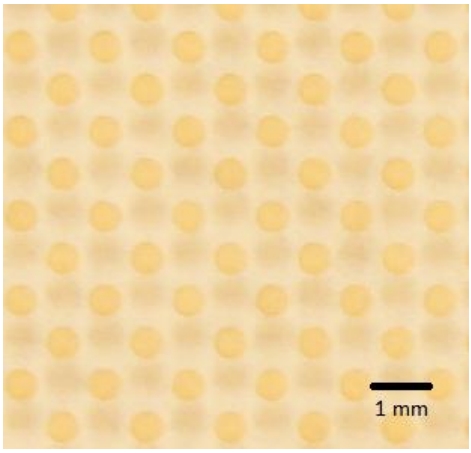

Figure 3.2: The top view photograph of AZ 40 XT photoresist-casted master mold. The diameters of the dots are 500 µm, and the spacing between dots is 1 mm. The depth of the master mold is 64 µm.

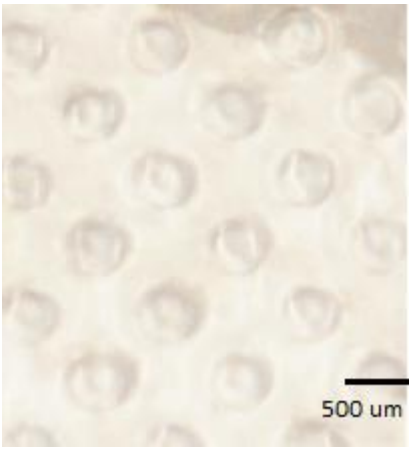

Figure 3.3: The top view photograph of PDMS sheet with holes created by the mold shown in Fig. 3.2.

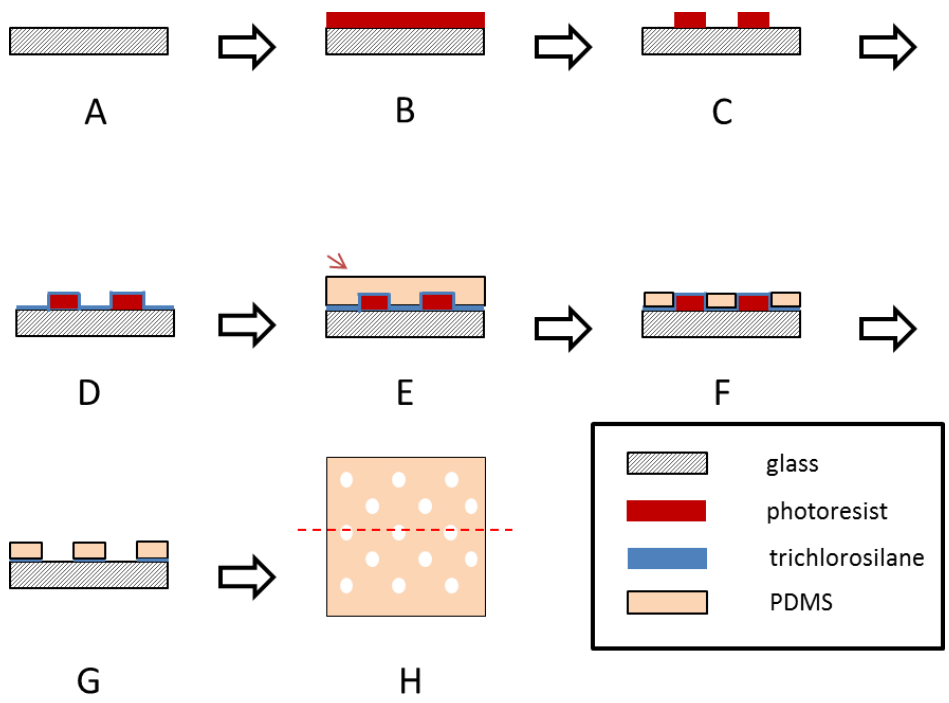

Figure 3.4: Schematic illustrations of fabrication procedures for molding PDMS. Frame A is a glass substrate. Fabrication procedures are provided from Frames B to G. (B) Spin-coating positive photoresist (C) Patterning positive photoresist in the form of trenches with layouts matching desired patterns. (D) Evaporating trichlorosilane on the surface of the photoresist mode. (E) Pouring 30:1 PDMS on the mold and scrapping gently with razor blade to remove excess PDMS. (F) Baking PDMS at 70 ºC oven for 2 hours to fully cure the polymer. (G)(H) Rinsing off the photoresist mold by acetone. (H) is the top view of finished PDMS sheet, and the red-dashed line shows the corresponding cross-sectioned view in (G).

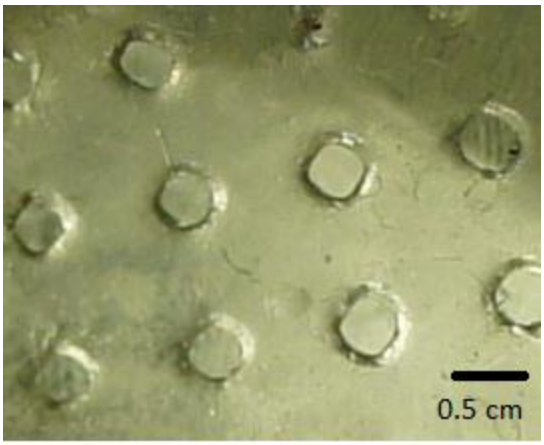

Figure 3.5: The top view photograph of PDMS sheet with hollows created by photopatternable PDMS.

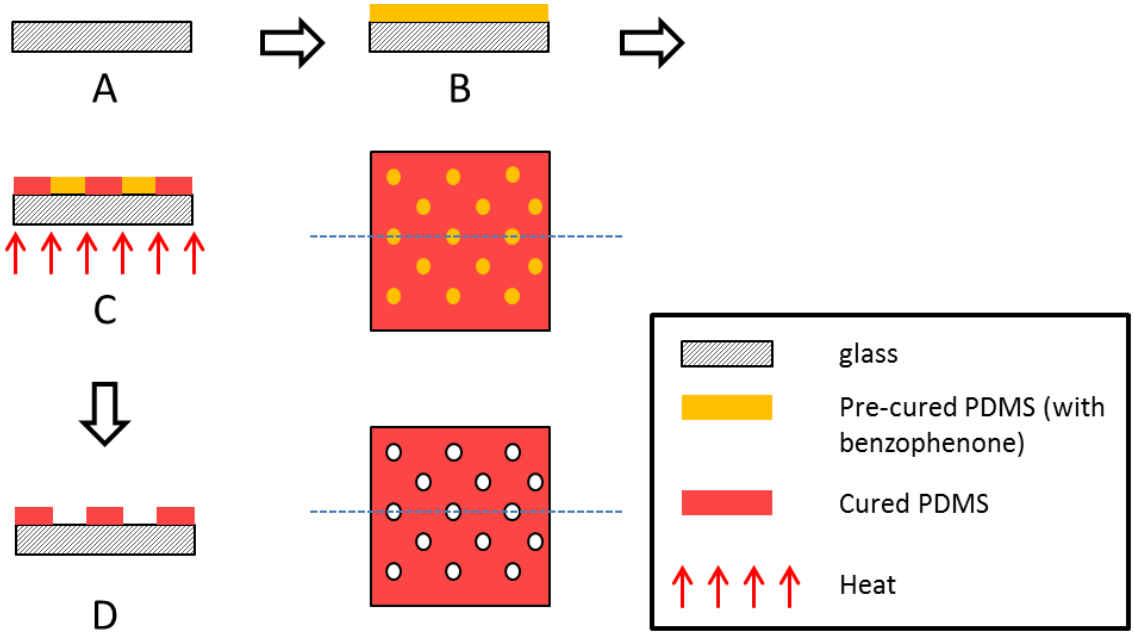

Figure 3.6: Schematic illustrations of fabrication procedures for molding PDMS. (A) A glass substrate. (B) Spin-coating pre-cured PDMS with benzophenone (like positive photoresist).(C) Exposing pre-cured PDMS under UV and baking at 110 ºC for 3 minutes to cure the part that was not exposed. The schematic on the right represents the top view of the PDMS and the blue dash line corresponds to the cross-section area shown in the left. (D) Removing the uncured part of PDMS by toluene. The schematic on the right represents the top view of the PDMS and the blue-dashed line corresponds to the cross-sectioned area shown in the left.

CHAPTER 4

EXPERIMENTAL SETUP

4.1 TENSILE TEST

By grabbing and stretching the sample on the Mini Instron, and collecting data with the previous mentioned USB multiemeter, the results are shown in Figure 4.1. Figure 4.1A shows an as-fabricated strain gauge composed of linear CB-PDMS resistors interconnected by serpentine CNT-PDMS conductors embedded in a transparent PDMS matrix. A deformed state (i.e. horizontal stretching to a strain of 150%) appears in Fig. 4.1B. Uniaxial tensile tests (Instron) with *in situ* electrical measurement allow evaluation of the *GF,* as shown in Fig. 4.1C. According to Eq. (6), the slope of the $(R-R_0)/R_0 \sim \varepsilon$ curve determines the *GF*. The results are 29.1 and (-4.9) for the longitudinal and lateral resistors, respectively. The negative *GF* is due to Poisson's effect, where lateral contraction occurs in conjunction with longitudinal elongation. Finite element models (FEM; ABAQUS CAE) for the strain fields reveal the underlying physics of deformation. Young's moduli obtained by uniaxial stress-strain curves (Fig. 4.1D) serve as input parameters, along with the detailed geometries. The measurements indicate that the Young's moduli for the CNT-PDMS, CB-PDMS and PDMS are 445 kPa, 275 kPa and 145 kPa respectively. The relative values of CNT-PDMS and CB-PDMS are consistent with the Guth [50] and Halpin–Tsai models [51], which predict that increasing the aspect ratio of the fillers increases the moduli. The effective modulus of the composite strain gauge sheet is 244 kPa, which lies within the range of values for the human epidermis, 140~600 kPa [52-54]. The symmetric and uniaxial tensile boundary conditions for the FEM are illustrated in Fig. 4.1E. A contour plot of

ε_{xx} for the integrated system appears in Fig. 4.1F, for the case of an applied strain of ε_{appl} = 10%. (By symmetry considerations, only the left half of the system was modeled.) The results show that while most of the PDMS matrix and the linear resistor structures experience a uniform strain of 10%, the average strain in the interconnects is only around 7%, where only ~30% of the interconnects experience strains higher than ~9%. This reduction results from the ability of the serpentine structures to undergo slight rigid body rotations to accommodate the applied stretch. Contour plots of longitudinal strain ε_{xx} and transverse strain ε_{yy} are plotted in Figs. 4.1G (without showing the PDMS matrix).

4.2 BENDING TEST

To test the devices in bending motion, I perform two types of tests. First, the sample sheet is rolled up and laminated on the outer surface of test tubes with different radius. Second, the sample sheet is attached to the human skin on the wrist and move with the wrist motion.

4.2.1 Test on Tubes

Strain gauges are responsive not only to tensile strains, but also to bending deformations and temperature changes. I performed experiments to explore these effects. Figure 4.2A presents a photograph of strain gauges wrapped around a cylindrical tube, as a representative setup for measuring the change of resistance as a function of the bending radius (black dots in Fig. 4.2B).

If I assume that the mechanical properties throughout the structure are approximately the same, then bending induced tensile strain along the outer surface of the structure is simply

$$\varepsilon = \frac{h}{2a} \tag{13}$$

where h is the sample thickness and a is the bending radius. The bending-induced change of resistance is, then,

$$\frac{(R - R_0)}{R_0} = GF \cdot \frac{h}{2a} \tag{14}$$

Equation (11) is plotted as the red dashed curve in Fig. 4.2B, which can properly capture the results of the bending experiment. Bending-induced strains are also verified through FEM as shown in Fig. 4.2C. When a 0.3-mm-thick sample is bent into a radius of 5 mm, Eq. (11) gives a bending strain of 3%, which matches well with the FEM result. To decouple bending-induced strain from tensile strain, I can intentionally place the CPDMS along a neutral mechanical plane by coating its surface with a layer of PDMS of identical thickness and stiffness with the underlying PDMS substrate. The change in resistance as a function of different bending radii for such a structure appears as blue dots in Fig. 4.2B, which indicates negligible strain due to pure bending.

4.2.2 Test on Wrist

For this reason, Wheatstone bridges serve as gauges for quantifying strains in human skin. Figure 4.3A plots the output voltage as a function of applied uniaxial tensile strain with an input voltage of 3 V. The change of output voltage is almost linear with strain. The output voltage as a

function of time under cyclic strain of up to 20% is plotted in Fig. 4.3B. Although CPDMS resistance under constant strain or stress may drift due to creep or relaxation [55], this time-dependence behavior is often reduced after cyclic loadings and hence hysteresis can also be minimized [24]. This type of elastomeric strain gauge sheet can be laminated onto the human wrist without fixtures or adhesives, as shown in Fig. 4.3C. The high compliance and thin geometry of the system are essential in avoiding slippage or detachment from the skin as the wrist is bent (Fig. 4.3C). These same properties minimize mechanical constraints on the natural motions of the skin, thereby ensuring that the measured strain reflects the actual deformation in skin. Corresponding measurements are provided in Fig. 4.3D. Voltage outputs from the Wheatstone bridge are fast and stable even under very quick repetitive motions. According to the voltage-strain ratio given by Fig. 4.3A and the amplitude in Fig. 4.3D, bending induced strain on the skin surface is between 11.2% to 22.6%, which is in good correspondence with the human skin deformability [56]. The strain gauge can be easily peeled off the skin after the measurements without causing any redness or irritation. Since the gauge remains intact after the cyclic test, it can be reused, and integrated onto other regions of the skin surface.

4.3 TEMPERATURE TEST

The effect of temperature can be explored both for an isolated resistor and a Wheatstone bridge configuration. The output voltage of a Wheatstone bridge (Fig. 1.2) is determined by (Eq.12). Changes in resistance of a resistor and the output voltage of a Wheatstone bridge appear as functions of temperature in Fig. 4.2D. Although the resistance of a single resistor

decreases significantly with temperature, the output voltage from the Wheatstone bridge is insensitive to temperature changes because the resistance of each resistor changes in the same manner, such that the ratios (Eq.18) remain invariant. This compensation mechanism makes Wheatstone bridge configurations attractive for accurate and stable strain sensing.

4.4 Figures

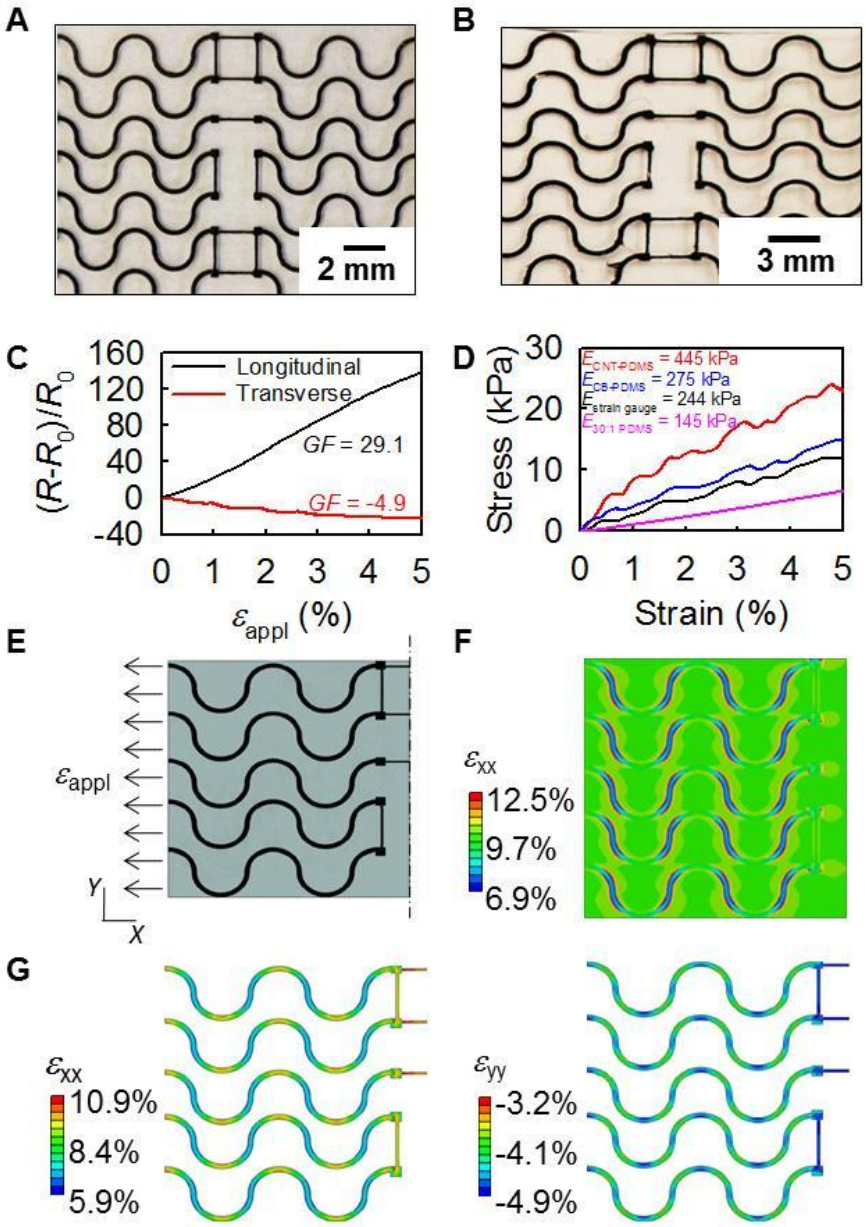

Figure 4.1: Tensile tests and finite element model (FEM) for all-elastomer strain gauges. (A) Top view of an as-fabricated strain gauge. (B) Top view of a strain gauge stretched by 150%. (C) Change of resistance for longitudinal and transverse resistors as a function of tensile strain. (D) Stress-strain curves and corresponding Young's moduli of the 30:1 PDMS matrix, CB-PDMS composite, CNT-PDMS composite and the strain gauge sample shown in Fig. 2A. (E) FEM model of the tensile test. (F) Contour plot of the longitudinal strain in both the PDMS substrate and the CPDMS devices. (G) Contour plot of the longitudinal strain in the CPDMS devices. (H) Contour plot of the transverse strain in the CPDMS devices.

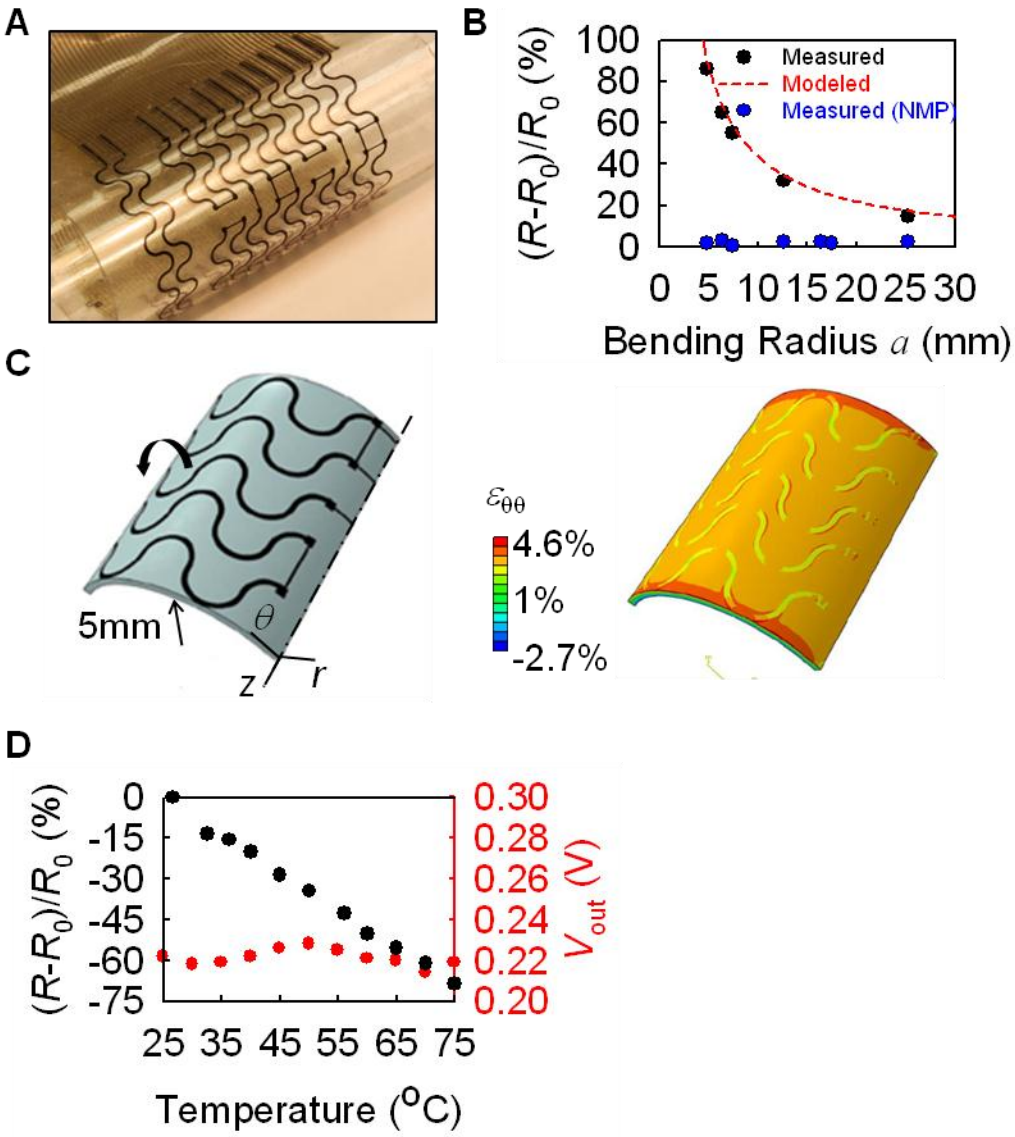

Figure 4.2: Calibration of bending and temperature effects of all-elastomer strain gauges. (A) Bending tests conducting by wrapping devices around cylinders with different radii. (B) Change in resistance as a function of bending radius. Black and blue dots are measured data for regular strain gauges and strain gauges placed along neutral mechanical plane respectively. The red dashed curve corresponds to an analytical model. (C) FEM of bending tests. The calculated strains match well with the analytical results. (D) Change of resistance of a resistor and change of output voltage of a Wheatstone bridge as functions of changes in temperature.

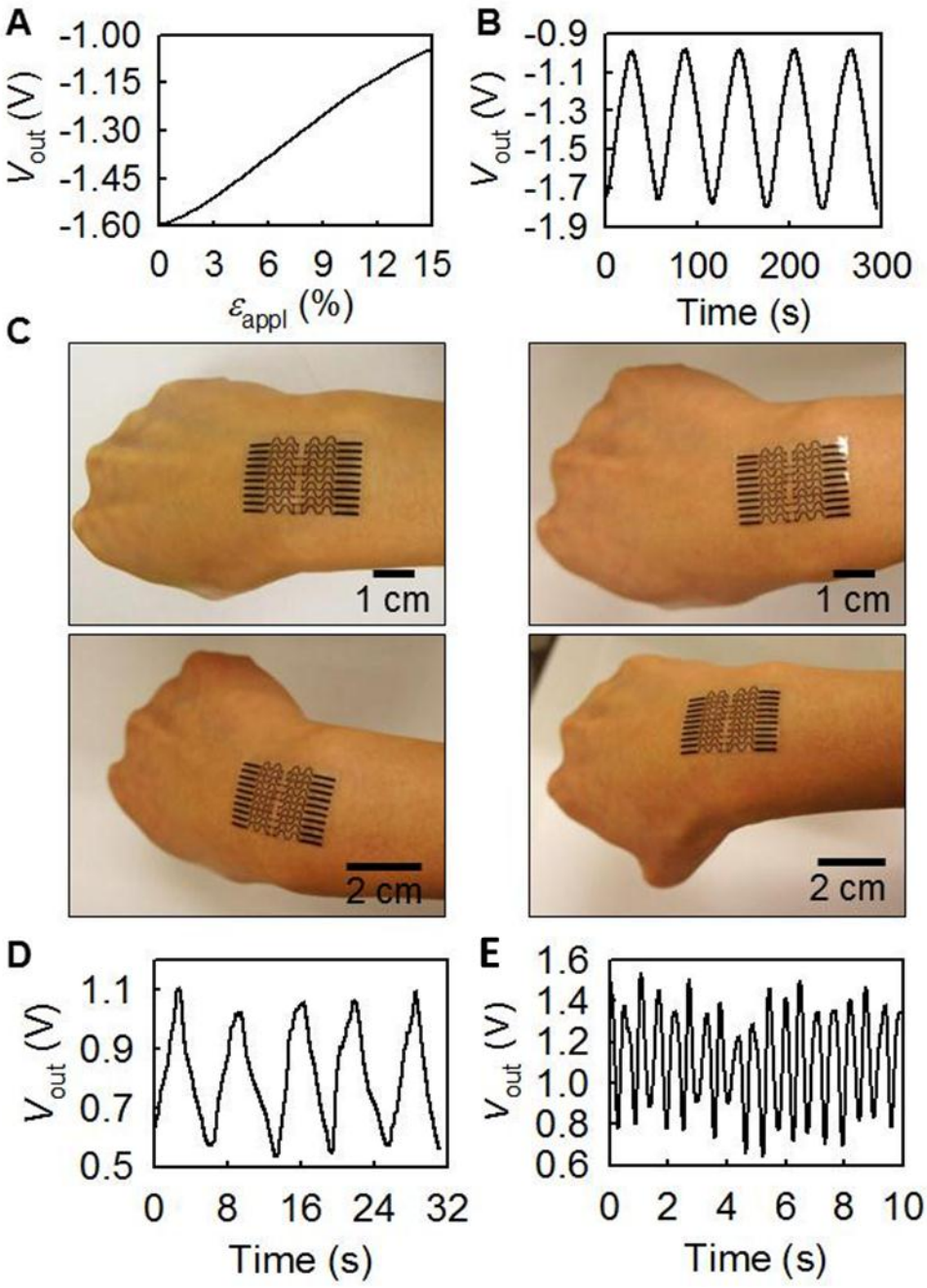

Figure 4.3: Using all-elastomer strain gauges in Wheatstone bridge configurations to quantify strain associated with deformations in human skin. (A) Output voltage as a function of uniaxial tensile strain. (B) Output voltage under cyclic stretching with maximum strain up to 30%. (C) Device laminated on the human wrist under various levels of bending. Output voltage when the wrist is undergoing (D) slow and (E) fast cyclic bending.

CHAPTER 5

MECHANICAL DESIGN AND ANALYSIS

5.1 MAIN GOALS OF DESIGN

Design considerations include sample thickness and stiffness, as well as accuracy in strain sensing. To minimize the overall stiffness, materials for both the matrix and the electrically active components should have low Young's moduli (ideally, comparable to the skin itself) and an ability to accommodate large strain deformations (~30% or more) with a linear, elastic response. Various features in the materials, mechanics and electrical transport properties are important. A typical device involves resistors (i.e. strain gauges) and conductors (i.e. electrical interconnect) connected in series, such that the change in resistance (ΔR) from an initial state (R_0) can be related, in a fractional sense, to the two individual components according to

$$\frac{\Delta R}{R_0} = \frac{\left(\Delta R_{\mathrm{r}} + \Delta R_{\mathrm{c}}\right)}{R_{\mathrm{r0}} + R_{\mathrm{c0}}} \tag{15}$$

where subscripts "r" and "c" denote resistor and conductor respectively. Applying Eq. (6) to each ΔR, yields

$$\frac{\Delta R}{R_0} = \frac{\left(GF_{\mathrm{r}}\varepsilon_{\mathrm{r}}R_{\mathrm{r0}} + GF_{\mathrm{c}}\varepsilon_{\mathrm{c}}R_{\mathrm{c0}}\right)}{R_{\mathrm{r0}} + R_{\mathrm{c0}}} \tag{16}.$$

A goal in mechanics and materials design is to configure the system such that the overall resistance change approaches the local resistance change of the resistor, i.e.

$$\frac{\Delta R_r}{R_{r0}} = GF_r \varepsilon_r \quad (17).$$

This outcome can be achieved by minimizing R_{c0}, GF_c, and ε_c. Since CB-PDMS has a much higher sheet resistance than CNT-PDMS at similar filler loading fractions [19], we use the former material for the sensors and the latter for the conductors, to yield $R_{c0} << R_{r0}$. Minimization of GF_c, requires consideration of two factors: the intrinsic material properties and the structure of the device. The intrinsic gauge factor of CPDMS itself is controlled by the type of filler and its loading fraction. The gauge factor of a structure of CPDMS has contributions from both the material and the geometry. Inspired by the shapes for metal interconnects in stretchable electronics [57-60], we exploited CNT-PDMS conductors in serpentine layouts, to minimize both the effective GF_c and ε_c.

5.2 MECHANICAL DESIGN

5.2.1 Serpentines

As highlighted by the FEM results, the *GF* not only depends on the materials, but also on the shape and associated mechanics of the conductor. For conductors of the same cross sectional dimensions and end-to-end lengths, the *GF* for strain applied along this length is twice as large for the linear case than it is for the serpentine structure, as illustrated in Fig. 5.1. The quantitative reason for this expected behavior is apparent from FEM shown in Fig. 5.1C. Under the same level of deformation, the strain in the linear conductors is uniform and comparable to the applied strain; non-uniform strain appears in the serpentine case, with maximum values that

are smaller than the applied strain. Since the system *GF* is defined as the resistance change per unit applied strain, the serpentine conductors have lower *GF* than linear ones.

A simple analytical model can capture this physics. Assume resistance is linearly proportional to length with a coefficient of β, and the gauge factor of a linear segment is GF_l, which is measured to be 0.52 for CNT-PDMS (Fig. 5.1B). The change of resistance of an infinitesimally short segment d*s* on an arbitrary curve, as shown in Fig. 5.1D, is given by

$$\mathrm{d}(\Delta R) = \beta \mathrm{d}s \cdot GF_l \cdot \frac{\mathrm{d}(\Delta s)}{\mathrm{d}s} \tag{18}.$$

Since $R_0 = \beta L_0$, we can write,

$$\frac{\mathrm{d}(\Delta R)}{R_0} = \frac{\beta GF_l \mathrm{d}(\Delta s)}{\beta L_0} \tag{19}.$$

Integration of both sides over the total length of the curve yields

$$\frac{\Delta R}{R_0} = GF_l \frac{\Delta L}{L_0} \tag{20},$$

which indicates the total change in resistance is proportional to the total change of the curve length. Since the serpentine shown in Fig. 5.1A is formed by interconnected half circles, the fractional change of the total length of a half circle after uniaxial stretch of ε_{appl} = 10% along the *x* axis (Fig. 5.1E) can be given by

$$\frac{\Delta L}{L_0} = \frac{\int_0^{\pi} r\sqrt{\sin^2\theta + (1.1\cos\theta)^2}\, d\theta - \pi r}{\pi r} = 0.051 \tag{21},$$

which is the same as the FEM output as shown in Fig. 5C. The effective gauge factor of the serpentine conductor can then be obtained analytically as,

$$GF_e = \frac{GF_l \frac{\Delta L}{L_0}}{\varepsilon_{\text{appl}}} = \frac{0.52 \times 0.051}{0.1} = 0.27 \quad (22),$$

which is in excellent agreement with the measured value of 0.28, as shown in Fig. 5.1B.

5.2.2 Thickness

In addition to the serpentine design of interconnects, the thicknesses and types of CPDMS used for the resistors and interconnects are different.

Resistance of device depends on not only the intrinsic properties of materials but also the cross section area of devices themselves. Therefore, one way to minimize the sensitivity of interconnect wires is to increase the cross section area of the wires; i.e. increase the thickness of the wires. For the device I present in this thesis, the thickness of the interconnect wires is around twice as thick as that of the resistors.

5.2.3 Types of Electrically Conductive Rubbers

Such behaviors, as well as the intrinsic differences between CNT-PDMS and CB-PDMS, can be observed in measurements on linear and serpentine CNT-PDMS with the same length, shown in Fig. 5.1A, with comparisons to the results of Fig. 4.1C. Figure 5.1B shows the change in resistance for the CNT-PDMS structures of Fig. 5.1A, as a function of the applied tensile strain. The initial resistance of the CNT-PDMS conductor is 0.31 kΩ which is ten times lower than that of a CB-PDMS resistor with even shorter length and higher filler loading: 4.13 kΩ, qualitatively consistent with literature reports [19, 26, 61, 62]. The low percolation threshold and

high conductivity in CNT-PDMS result from its unique filler geometry. The *GF* for CNT-PDMS (0.52) is also lower than that for CB-PDMS (29.1). When CB-PDMS is elongated, the conducting carbon particles can easily separate, resulting in breaking of conductive pathways and therefore, significant increases in resistance. In contrast, CNTs may rotate and/or slide against each other to accommodate applied deformations. In this way, a significant fraction of the networks can remain connected and conductive, hence resulting in reduced changes in resistance [61]. For these two reasons (i.e. low resistance and low *GF*), CNT-PDMS is more suitable than CB-PDMS as the interconnects; the opposite is the case for the sensors.

5.3 Figures

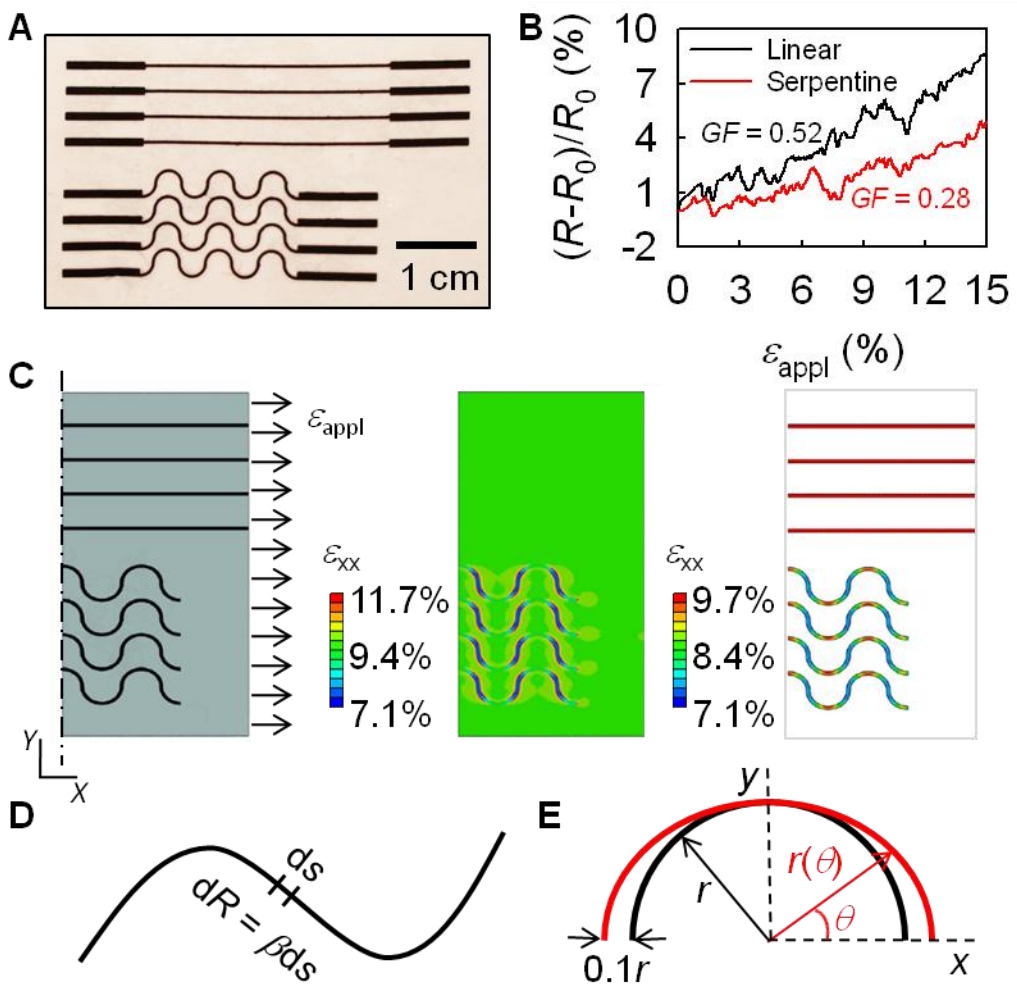

Figure 5.1: Comparison of linear and serpentine structures of CNT-PDMS. (A) Top view of as-fabricated linear and serpentine structures of CNT-PDMS embedded in a PDMS substrate. (B) Change in resistance of linear and serpentine structures of CNT-PDMS as a function of applied tensile strain. (C) FEM model of the tensile test. (D) Illustration of an infinitesimally short segment on an arbitrarily shaped curve, for analytical calculation. (E) Illustration of a half circle stretched by 10% along *x* axis, for analytical calculation.

CHAPTER 6

CONCLUSIONS AND FUTURE DIRECTIONS

6.1 CONCLUSIONS

In summary, all-elastomer, highly sensitive strain gauges can be fabricated by molding processes with two types of conducting elastomers, all integrated in a third, insulating elastomer. Demonstration experiments and calculations illuminate all of the key mechanical and material aspects of these systems; use on the human skin illustrates their operation. Particularly when integrated with stretchable electronics and other classes of sensors, these technologies have the potential to expand the range of function that can be achieved in bio-integrated systems, with potential utility in wound monitoring, human-machine interfaces, and others.

6.2 FUTURE DIRECTIONS

Currently, the fabrication and testing procedures are very repeatable, and the performance of devices (resistors and Wheatstone bridges) is very stable and reliable. However, bonding ACF ribbons to the interconnect pads will be an unnecessary process if there is an antenna integrated into the device and if there is a wireless receiver. In this case, the weight of the device can be scaled down significantly since the weight of device itself is very light.

Moreover, without the ACF ribbons, this highly sensitive strain gauge based entirely on elastomers can be wearable, and it will be much more convenient for measurements.

In addition, the resistors or Wheatstone bridges can be made into an array so that the circuit can be applied to map out the motion over an area. Nevertheless, this requires not only the upgrade in the device but also an upgrade on the data acquisition system. All the data acquired and reported here in this thesis were measured separately. It would have been challenging to measure multi-channels at the same time for the resistors (made of CB-PDMS) that I report here due to the fact that their resistance is extremely high (in the range of MOhm). If these problems can be solved, then the application of all-elastomer strain gauges can be more versatile.

REFERENCES

[1] Sohn H., Farrar C.R., Hunter N.F., et al., **2001**, *Journal of Dynamic Systems Measurement and Control-Transaction of The ASME*, 123(4), 706-711.

[2] Szivek J.A., Roberto R.F., Slack J.M., et al., **2002**, SPINE, 27(5): p. 487-497

[3] *Strain Rosette for Strain Measurement*, Dec. 18th 2010, Available from: http://www.efunda.com/formulae/solid_mechanics/mat_mechanics/strain_gage_rosette.cfm

[4] A. L. Window, *Strain gauge technology*, Elsevier Applied Science, London, England **1992**.

[5] N. Lu, X. Wang, Z. Suo, J. Vlassak, **2007**, *Appl. Phys. Lett., 91*, 221909.

[6] C. S. Smith, **1954**, *Phys. Rev., 94*, 42.

[7] S. M. Sze, *Semiconductor Sensors*, Wiley, New York **1994**.

[8] A. A. Barlian, W. Park, J. R. Mallon Jr., A. J. Rastegar, B. L. Pruitt, **2009**, *Proc IEEE, 97*, 513.

[9] Y. Kanda, **1991**, *Sensors and Actuators A-Physical, 28*, 83.

[10] S. Middlehoek, S. A. Audet, *Silicon Sensors*, Delft University Press, Delft, The Netherlands **1994**.

[11] J. A. Rogers, M. G. Lagally, R. G. Nuzzo, **2011**, *Nature*, *477*, 45.

[12] Sang Min Won, Hoon-sik Kim, Nanshu Lu, Dae-gon Kim, Cesar Del Solar, Terrisa Duenas, Abid Ameen, John A. Rogers, **2011**, *IEEE Transactions on Electron Devices*.

[13] E. Chao, K. An, L. Askew, B. Morrey, **1980**, *Journal of Biomechanical Engineering-Transactions of the Asme, 102*, 301.

[14] K. Rome, F. Cowieson, **1996**, *Foot & Ankle International, 17*, 28.

[15] G. Bell, P. Nielsen, N. Lassen, B. Wolfson, **1973**, *Cardiovasc. Res., 7*, 282.

[16] M. Leonardi, E. M. Pitchon, A. Bertsch, P. Renaud, A. Mermoud, **2009**, *Acta Ophthalmol., 87*, 433.

[17] D. Kim, N. Lu, R. Ma, Y. Kim, R. Kim, S. Wang, J. Wu, S. M. Won, H. Tao, A. Islam, K. J. Yu, T. Kim, R. Chowdhury, M. Ying, L. Xu, M. Li, H. Chung, H. Keum, M. McCormick, P. Liu, Y. Zhang, F. G. Omenetto, Y. Huang, T. Coleman, J. A. Rogers, **2011**, *Science, 333*, 838.

[18] T. Yamada, Y. Hayamizu, Y. Yamamoto, Y. Yomogida, A. Izadi-Najafabadi, D. N. Futaba, K. Hata, **2011**, *Nature Nanotechnology, 6*, 296.

[19] C. Liu, **2007**, *Adv Mater, 19*, 3783.

[20] S. R. Quake, A. Scherer, **2000**, *Science, 290*, 1536.

[21] S. Rwei, F. Ku, K. Cheng, **2002**, *Colloid Polym. Sci., 280*, 1110.

[22] X. Niu, S. Peng, L. Liu, W. Wen, P. Sheng, **2007**, *Adv Mater, 19*, 2682.

[23] K. S. Ryu, X. Wang, K. Shaikh, C. Liu, **2004**, *Microelectromechanical Systems, Journal of, 13*, 568.

[24] D. Kim, N. Lu, R. Ghaffari, Y. Kim, S. P. Lee, L. Xu, J. Wu, R. Kim, J. Song, Z. Liu, J. Viventi, B. de Graff, B. Elolampi, M. Mansour, M. J. Slepian, S. Hwang, J. D. Moss, S. Won, Y. Huang, B. Litt, J. A. Rogers, **2011**, *Nature Materials, 10*, 316.

[25] A. Medali, **1986**, *Rubber Chemistry and Technology, 59*, 432.

[26] L. Bokobza, **2007**, *Polymer, 48*, 4907.

[27] P. Pramanik, D. Khastgir, S. De, T. Saha, **1990**, *J. Mater. Sci., 25*, 3848.

[28] A. Celzard, E. McRae, C. Deleuze, M. Dufort, G. Furdin, J. Mareche, **1996**, *Physical Review B, 53*, 6209.

[29] M. Taya, W. Kim, K. Ono, **1998**, *Mech. Mater., 28*, 53.

[30] T. Someya, T. Sekitani, S. Iba, Y. Kato, H. Kawaguchi, T. Sakurai, **2004**, *Proc. Natl. Acad. Sci. U. S. A., 101*, 9966.

[31] K. Takei, T. Takahashi, J. C. Ho, H. Ko, A. G. Gillies, P. W. Leu, R. S. Fearing, A. Javey, **2010**, *Nature Materials, 9*, 821.

[32] L. Chen, G. Chen, L. Lu, **2007**, *Advanced Functional Materials, 17*, 898.

[33] Ching-Hsiang Cheng, Lidan Xiao, Yin-Nee Cheung, Chen Chao, Mo Yang, King-Lun Kwok, Po-Fat Chong, W. Leung, "A strain gauge that uses carbon black and carbon nanotube doped silicone oil encapsulated in a PDMS microchannel", presented at Nanotechnology, **2007**. IEEE-NANO 2007. 7th IEEE Conference on 2007.

[34] A. R. Aiyar, C. Song, S. Kim, M. G. Allen, **2009**, *Smart Materials & Structures, 18*, 115002.

[35] S. K. Sia, G. M. Whitesides, Electrophoresis 2003, 24, 3563.

[36] B. H. Jo, L. M. V. Lerberghe, K.M. Motsegood, D. J. Beebe, JMEMS 2000, 9, 76.

[37] J. H. Ward, R. Bashir, N. A. Peppas, J. Biomed. Mater. Res. 2001, 56,351.

[38] J. C. Lotters, W. Olthuis, P. H. Veltink, P. Bergveld, J. Micromech. Microeng. 1997, 7, 145.

[39] M. Almasri, W. Zhang, A. Kine, Y. Chan, J. C. LaRue, R. Nelson, Proc. SPIE 2005, 5770, 190.

[40] C. Iojoiu,M. Ropot,M. J.M. Abadie, V. Harabagiu,M. Pinteala, B. C. Simionescu, Sci. Isr. – Technol. Adv. 2000, 36, 2115.

[41] H. Cong, Tingrui Pan, 2008, *Adv Fun Mater,* 18, 1912

[42] Patternable Silicones for Electronics, Product Data Sheet, Dow Corning 2005.

[43] B. Harkness, G. Gardner, J. Alger, M. Cummings, J. Princing, Y. Lee, H. Meynen, M. Gonzalez, B. Vandevelde, M. V. Bulcke, C. Winters, E. Beyne, Proc. SPIE 2004, 5376, 517.

[44] G. Gardner, B. Harkness, E. Ohare, H. Meynen, M. Bulcke, M. Gonzalez, E. Beyne, Proceedings of the 54th Electronic Components and Technology Conference, Las Vegas, NV 2004.

[45] A. A. S. Bhagat, P. Jothimuthu, I. Papautsky, Lab Chip 2007, 7, 1192.

[46] L. Pouliquen, X. Coqueret, Macromol. Chem. Phys. 1996, 197, 4045.

[47] U. Muller, H. J. Tempet, N. Neuegufeld, Eur. Polym. J. 1991, 27, 621.

[48] U. Muller, S. Jockusch, H. J. Timpe, J. Polym. Sci, Part A: Polym. Chem. 1992, 30, 2755.

[49] K. Tsougeni, A. Tserepi, E. Gogolides, Microelectron. Eng. 2007, 84, 1104.

[50] E. Guth, **1945**, *J. Appl. Phys.*, *16*, 1707495.

[51] J. Halpin, **1969**, *J. Composite Mater.*, *3*, 732.

[52] C. Pailler-Mattei, S. Bec, H. Zahouani, **2008**, *Med. Eng. Phys.*, *30*, 599.

[53] O. Kuwazuru, J. Saothong, N. Yoshikawa, **2008**, *Med. Eng. Phys.*, *30*, 516.

[54] M. Geerligs, L. van Breemen, G. Peters, P. Ackermans, F. Baaijens, C. Oomens, **2011**, *J. Biomech.*, *44*, 1176.

[55] M. Shimojo, A. Namiki, M. Ishikawa, R. Makino, K. Mabuchi, **2004**, *Sensors Journal, IEEE*, *4*, 589.

[56] V. Arumugam, M. Naresh, R. Sanjeevi, **1994**, *J. Biosci.*, *19*, 307. .

[57] D. Gray, J. Tien, C. Chen, 2004, Adv Mater, 16, 393.

[58] T. Li, Z. G. Suo, S. P. Lacour, S. Wagner, 2005, Journal of Materials Research, 20, 3274.

[59] D. Kim, J. Song, W. M. Choi, H. Kim, R. Kim, Z. Liu, Y. Y. Huang, K. Hwang, Y. Zhang, J. A. Rogers, 2008, Proc. Natl. Acad. Sci. U. S. A., 105, 18675.

[60] M. Gonzalez, F. Axisa, M. V. BuIcke, D. Brosteaux, B. Vandevelde, J. Vanfleteren, 2008, Microelectronics Reliability, 48, 825.

[61] L. Flandin, A. Chang, S. Nazarenko, A. Hiltner, E. Baer, **2000**, *J Appl Polym Sci, 76*, 894.

[62] W. Thongruang, C. Balik, R. Spontak, **2002**, *Journal of Polymer Science Part B-Polymer Physics, 40*, 1013.